# Predictive direct torque control with reduced ripples for induction motor drive based on T-S fuzzy speed controller

Abdelkarim Ammar, Billel Talbi, Tarek Ameid, Younes Azzoug, Abdelaziz Kerrache

# Predictive direct torque control with reduced ripples for induction motor drive based on T-S fuzzy speed controller

Abdelkarim Ammar[1,4] | Billel Talbi[2] | Tarek Ameid[3] | Younes Azzoug[3,4] | Abdelaziz Kerrache[5]

[1]Signals and Systems Laboratory (LSS), Institute of Electrical and Electronic Engineering, University of Boumerdes, Boumerdes, Algeria

[2]Laboratory of Power Electronics and Industrial Control, University of Sétif 1, Sétif, Algeria

[3]Faculty of Applied Science, University of Artois, Béthune, France

[4]Electrical Engineering Laboratory of Biskra (LGEB), University of Biskra, Biskra, Algeria

[5]Electrical Engineering Laboratory of ENP (LRE) National Polytechnic School, Algiers, Algeria

**Abstract**

Finite-state model predictive control (FS-MPC) has been widely used for controlling power converters and electric drives. Predictive torque control strategy (PTC) evaluates flux and torque in a cost function to generate an optimal inverter switching state in a sampling period. However, the existing PTC method relies on a traditional proportional-integral (PI) controller in the external loop for speed regulation. Consequently, the torque reference may not be generated properly, especially when a sudden variation of load or inertia takes place. This paper proposes an enhanced predictive torque control scheme. A Takagi-Sugeno fuzzy logic controller replaces PI in the external loop for speed regulation. Besides, the proposed controller generates a proper torque reference since it plays an important role in cost function design. This improvement ensures accurate tracking and robust control against different uncertainties. The effectiveness of the presented algorithms is investigated by simulation and experimental validation using MATLAB/Simulink with dSpace 1104 real-time interface.

**KEYWORDS**

direct torque control (DTC), dSpace 1104, induction motor (IM), predictive torque control (PTC), Takagi-Sugeno fuzzy logic controller (TS-FLC)

## 1 | INTRODUCTION

The development of direct torque control (DTC) has offered many advantages, such as simple structure and fast response [1]. However, the presence of high ripples and current harmonics due to the use of hysteresis comparators diminishes the performance of a controlled machine, especially at low-speed. Several methods have been introduced recently to overcome the drawbacks of the traditional DTC. Nowadays, model predictive control (MPC) has attracted the attention of researchers in power electronics and electrical drives field [2]. MPC uses the dynamic model of the controlled process within the controller to anticipate in real-time the future behavior of the process [3]. The model predictive control in the electrical drives field can be divided into continuous state and finite-state model predictive control. The continuous MPC can achieve good performance, but it has a complicated structure and requires a pulse width modulator unit (PWM) to control the power converter [4]. Whilst, the finite-state MPC does not need a modulation unit, it incorporates instead the converters model in the control design with respect to its discrete nature [5]. Then, the switching states are considered to minimize a predefined

cost function in order to select the optimal voltage vector for the next sampling period.

In the context of AC machines drive, several model predictive-based strategies have arisen [2,6]. Predictive torque control (PTC) has a similar basic structure as DTC, where the hysteresis controllers and the switching table are replaced by an online optimization procedure [7]. In this strategy, the torque and the stator flux are predicted for the finite number of possible switching states of the voltage source inverter. Then, the selected states by actuating the cost function will be applied directly to the inverter in the next sampling instant. The optimal choice of switching states can reduce torque and flux ripples and improve the current quality, which overcomes the main DTC drawback [8].

In spite of the breakthrough advancement in the finite-state model predictive control, the proportional-integral controller is still commonly used for speed control in the outer loop [9]. However, the PI may not operate well and degrades dynamic performance in the presence of disturbances and uncertainties. In addition, PI controller gains are usually designed using a poles placement approach, which requires the exact knowledge of the mathematical model and its parameters. Therefore, this issue raises concerns about robustness and disturbance rejection ability. Since a high-performance controller like FS-MPC is used in the main control scheme, it is highly recommended to join it with a robust controller in the outer speed loop to achieve comprehensive enhancement, [10].

Several control methods have been proposed to improve the robustness of the speed loop. Those mentioned in the literature include nonlinear control approaches and artificial intelligence techniques [11,12]. Artificial intelligence methodologies have emerged recently as promising ways to solve nonlinear, uncertain, and complex systems [13]. In particular, fuzzy logic (FLC) can offer a fast response and accurate tracking in the speed loop without requiring knowledge of the mathematical model. The Mamdani type based-FLC has been applied widely in electrical drives, giving satisfactory results [14]. However, its main shortcoming is the need for a big number of fuzzy sets to achieve an acceptable level of performance. On the other hand, Takagi-Sugeno type based fuzzy logic offers an easier structure and simpler design [15]. Besides, it is very suitable for use in nonlinear systems and gives good performance with fewer inference rules.

Therefore, the main objective of this work is to improve the external speed loop of the finite-state predictive control for induction motor drive using a Takagi-Sugeno fuzzy logic controller (TS-FLC). The latter can drive the rotor speed accurately and shows high robustness against parameter variations and different uncertainties. Besides, TS-FLC generates faster and more precise torque reference for cost function optimization, which can be very helpful to ensure comprehensive PTC performance enhancement, especially in the presence of load disturbance. The presented methods will be investigated through simulation and experimental verification using MATLAB/Simulink with dSpace 1104 board.

## 2 | FINITE-STATE PREDICTIVE TORQUE CONTROL

### 2.1 | IM model

The dynamic model of the induction machine is expressed in the stationary reference frame. (1), (2), and (3) present voltage and flux equations and torque expression respectively:

$$\begin{cases} \bar{v}_s = R_s \bar{i}_s + \dfrac{d\bar{\psi}_s}{dt} \\ 0 = R_r \bar{i}_r + \dfrac{d\bar{\psi}_r}{dt} - j\omega_r \bar{\psi}_r \end{cases} \tag{1}$$

$$\begin{cases} \bar{\psi}_s = L_s \bar{i}_s + M_{sr} \bar{i}_r \\ \bar{\psi}_r = M_{sr} \bar{i}_s + L_r \bar{i}_r \end{cases} \tag{2}$$

$$T_e = p \cdot \mathrm{Im}\{\bar{\psi}_s \cdot \bar{i}_s\} \tag{3}$$

With

$\bar{i}_s$ and $\bar{i}_r$ are stator and rotor current vectors respectively.

$\bar{v}_s$ is stator voltage vector.

$\bar{\psi}_s$ and $\bar{\psi}_r$ are stator and rotor flux vectors respectively.

$R_s$ and $R_r$ are stator and rotor phase resistances respectively.

$L_s$ and $L_r$ are stator and rotor phase inductances respectively.

$M_{sr}$ is stator-rotor mutual inductance.

$\omega_r$ is angular velocity.

$p$ is number of pole pairs.

### 2.2 | Stator current, flux, and electromagnetic prediction

After the estimation of flux and torque using the machine model, the next step in the predictive torque control

algorithm is the prediction of the next-instant of current $\bar{i}_s(k+1)$, flux, $\widehat{\bar{\psi}}_s(k+1)$, and torque $\widehat{T}_e(k+1)$.

The stator current and the stator flux can be described as follows:

$$\frac{d\widehat{\bar{\psi}}_s}{dt} = \bar{v}_s - R_s\bar{i}_s \tag{4}$$

$$\bar{i}_s = -\frac{1}{R_\sigma}\left(L_\sigma \cdot \frac{d\bar{i}_s}{dt} - k_r \cdot \left(\frac{1}{T_r} - j\omega\right)\bar{\psi}_r\right) - \bar{v}_s \tag{5}$$

where:

$$k_r = M_{sr}/L_r,\ R_\sigma = R_s + k_r^2 \cdot R_r,\quad \sigma = 1 - \frac{M_{sr}}{L_s L_r},\quad L_\sigma = \sigma . L_s$$

To predict the next instants of currents, flux and torque, the Euler forward discretization is used:

$$\frac{dx}{dt} \approx \frac{x(k+1) - x(k)}{T_z} \tag{6}$$

After the discretization with the sampling time $T_z$, the stator flux prediction can be obtained as:

$$\widehat{\bar{\psi}}_s(k+1) = \widehat{\bar{\psi}}_s(k) + T_z\bar{v}_s(k) - R_s \cdot T_z\bar{i}_s(k) \tag{7}$$

The stator current prediction can be obtained as:

$$\bar{i}_s(k+1) = \left(1 - \frac{T_z}{T_\sigma}\right) \cdot \bar{i}_s(k) + \frac{T_z}{T_\sigma} \cdot \frac{1}{R_\sigma}$$

$$\left(k_r \cdot \left(\frac{1}{T_r} - j\omega(k)\right)\bar{\psi}_r(k) + \bar{v}_s(k)\right) \tag{8}$$

with

$$T_\sigma = \sigma L_s/R_\sigma$$

By the predictions of the stator flux and current, the torque can be predicted as follows:

$$\widehat{T}_e(k+1) = p \cdot \mathrm{Im}\left\{\widehat{\bar{\psi}}_s(k+1) \cdot \bar{i}_s(k+1)\right\} \tag{9}$$

## 2.3 | Voltage vector selection

Eight possible vectors can be obtained from the combinations of two-level inverter switching states, six are active vectors (*V1, V2 ... V6*) and two are zero vectors (*V0, V7*).

The third step in the PTC algorithm is voltage vector selection through the cost function optimization. The cost function compares the reference values of the torque and the flux with the predicted values. The considered cost function in this work is expressed as follows:

$$g = \frac{1}{T_{en}^2}\left|T_e^* - \widehat{T}_e(k+1)\right| + \frac{\lambda}{\psi_{sn}^2}\left|\bar{\psi}_s^* - \widehat{\bar{\psi}}_s(k+1)\right| + I_{\lim} \tag{10}$$

where

$T_e^*$ and $\bar{\psi}_s^*$ are the reference values of torque and flux respectively.

$T_{en}$ and $\psi_{sn}$ are the rated values of the torque and flux respectively.

$\lambda$ is the weighting factor.

$I_{\lim}$ is a current limitation term added in order to protect the system from the overcurrent. This term is designed according to the maximum supportable current $i_{max}$ by the machine [16].

$$I_{\lim} = \begin{cases} \infty,\ if\left|\bar{i}_s(k+1)\right| > i_{\max} \\ 0,\ if\left|\bar{i}_s(k+1)\right| \le i_{\max} \end{cases} \tag{11}$$

# 3 | TAKAGI-SUGENO FUZZY LOGIC-SPEED CONTROLLER DESIGN

Fuzzy logic control is mostly used for high uncertainty nonlinear systems. In this section, a Takagi-Sugeno fuzzy logic controller is designed for speed regulation and reference torque generation to improve the performance of a PTC control scheme. The T-S method requires the least computation effort compared to other fuzzy inference methods [17]. The zero-order TS-FLC is composed of three basic processes as shown in Figure 1: fuzzification, rules base, and defuzzification [18].

$K_e$, $K_{\Delta e}$ and $K_u$ are the normalization factors.

The selection of input and output normalization factors is made based on the knowledge about the process.

$e(k)$is the rotor speed tracking error.

Figures 2–3 represent the proposed normalized input and output membership functions in terms of linguistic variables, NB (Negative Big), NM (Negative Medium),

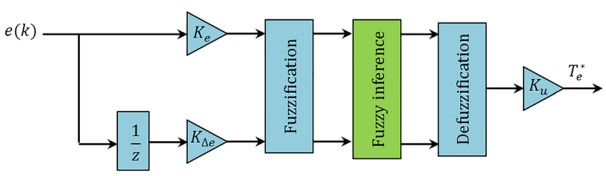


**FIGURE 1** Block diagram of the proposed FLC [Color figure can be viewed at wileyonlinelibrary.com]

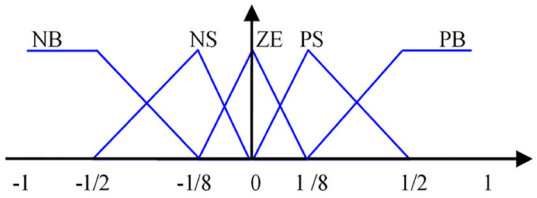


**FIGURE 2** TS-FLC inputs membership functions [Color figure can be viewed at wileyonlinelibrary.com]

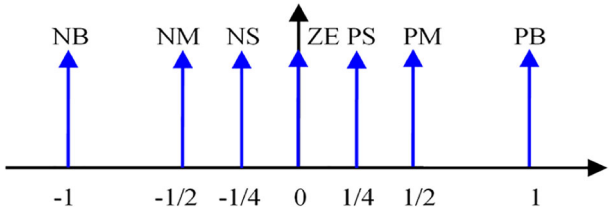


**FIGURE 3** TS-FLC output membership functions [Color figure can be viewed at wileyonlinelibrary.com]

NS (Negative Small), ZE (Zero), PS (Positive Small), PM (Positive Medium), and PB (Positive Big). In the last step, a center weighted average algorithm is used in the defuzzification process.

The fuzzy rules used in the proposed FLC can be represented in a symmetric form, as illustrated in Table 1.

Figure 4 shows the global diagram of predictive direct torque control associated to TS fuzzy logic speed controller.

## 4 | SIMULATION RESULTS

The simulation results were obtained using MATLAB/Simulink software, and the characteristics of the induction motor are given in the appendix. The simulation results are presented in three sections: a comparative study between the finite state predictive torque control (FS-PTC) and the conventional direct torque control using switching table (ST-DTC), then, a robustness test of resistance variation. The last section presents the comparative analysis of the speed controllers in the external loop (i.e., PI and Takagi-Sugeno fuzzy logic controller TS-FLC).

**TABLE 1** Fuzzy rules base

| | $e(k)$ | | | | |
|---|---|---|---|---|---|
| $\Delta e(k)$ | **NB** | **NS** | **ZE** | **PS** | **PB** |
| NB | NB | NB | NM | NS | ZE |
| NS | NB | NM | NS | ZE | PS |
| ZE | NM | NS | ZE | PS | PM |
| PS | NS | ZE | PS | PM | PB |
| PB | ZE | PS | PM | PB | PB |

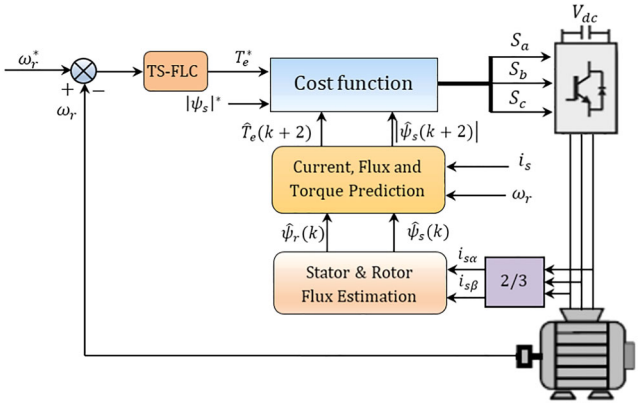


**FIGURE 4** Block diagram of predictive torque control with T-S fuzzy logic speed controller for IM drive [Color figure can be viewed at wileyonlinelibrary.com]

### 4.1 | Conventional DTC and PTC comparative analysis

Different operation conditions have been performed to check the effectiveness of control schemes, such as: steady state, speed sense reversal, and load application. The following Figures are specified (a) for switching table-based DTC (ST-DTC) and (b) for predictive torque control (PTC).

In order to check control performance in different operation points, Figure 5 (a)–(b) presents the rotor speed and torque during speed reversal maneuver without load. Both control algorithms have a good dynamic in the steady state, however, DTC shows high torque ripples in Figure 5(a) contrary to the PTC in Figure 5(b), which has a reduced ripple level. Then, Figure 6(a)–(b) presents flux magnitude and components. Figure 6 shows that PTC has a lower flux ripple and good waveform compared to ST-DTC. Therefore, it can be deduced that PTC solves the main drawbacks of DTC.

Next, Figure 7 illustrates the load application test. Despite both control strategies showing a good loading ability, it can be observed that PTC in Figure 7(b) has better current quality and reduced harmonics due to the optimal selection of voltage vectors. Next, the current spectrum of total harmonics distortion (THD) has been displayed in Figure 8. It can be observed that PTC provided better current quality and lower current THD (7.94%), unlike DTC, which shows an important current THD (13.84%). Finally, in Figure 9, a low-speed operation test of *200 rpm* (*20.93 rad/s*) has been conducted. The figures show, from top to bottom, rotor speed, torque, and stator current. In Figure 9(a), DTC shows some speed fluctuations and high torque ripples (±1 N.m) and current harmonics. In contrast, PTC has reducer torque ripples (±0.4 N.m) and a smoother current waveform.

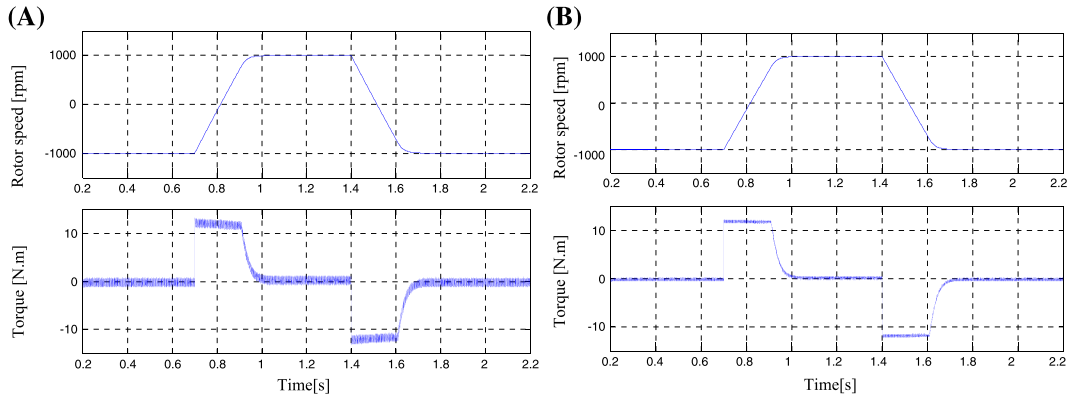


**FIGURE 5** Rotor speed [rpm], electromagnetic torque [N.m] during the speed reversal. **A**, for DTC. **B**, for PTC [Color figure can be viewed at wileyonlinelibrary.com]

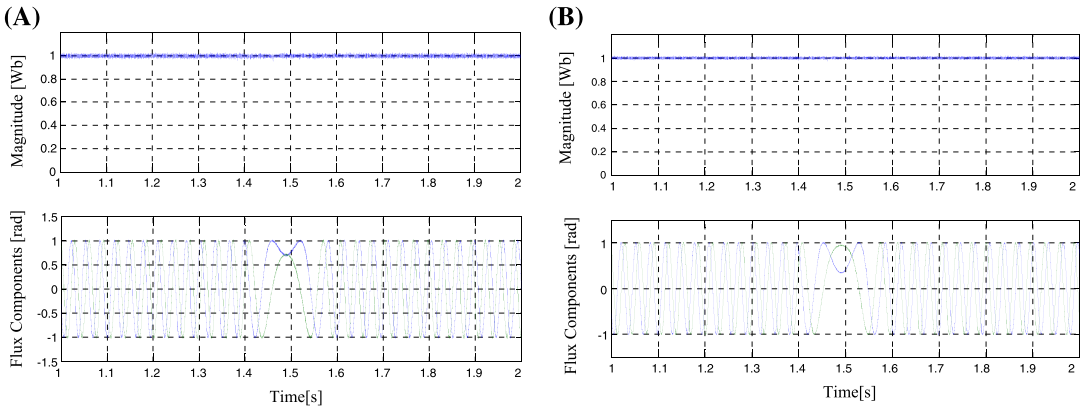


**FIGURE 6** Stator flux magnitude [Wb], stator flux components [Wb] during the speed reversal. **A**, for DTC. **B**, for PTC [Color figure can be viewed at wileyonlinelibrary.com]

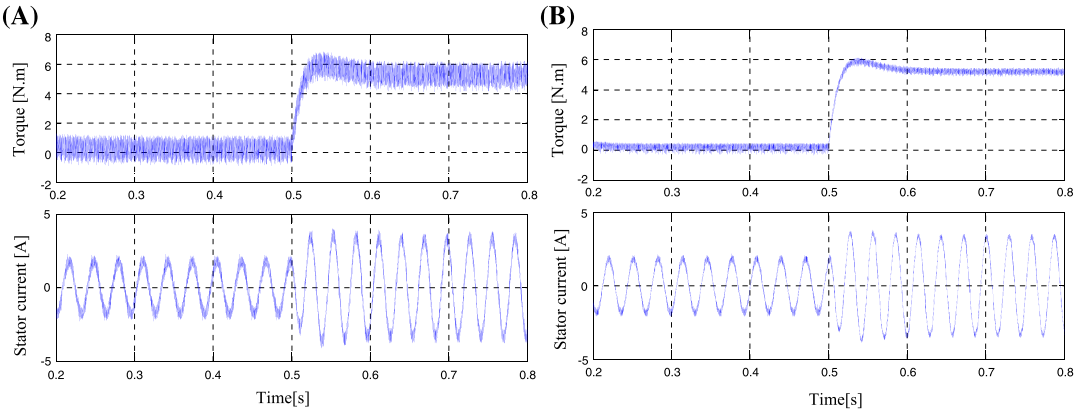


**FIGURE 7** Electromagnetic torque [N.m] and stator phase current [a] with load application of 5 N.m. **A**, for DTC. **B**, for PTC [Color figure can be viewed at wileyonlinelibrary.com]

## 4.2 | Parameters variation robustness test

This test has been conducted as a simulation study in order to check the ability of both control techniques with the variation of parameters. It consists of increasing the stator resistance $R_s$ when the machine operates with very low speed (*20 rpm* ≈ *2.09 rad/s*). $R_s$ increases by 50% starting from 0.1 s.

Figure 10 illustrates flux magnitude and rotor speed. It is observed that the flux estimation accuracy and the speed responses of DTC and PTC have been influenced owing to the large influence of the stator resistance in

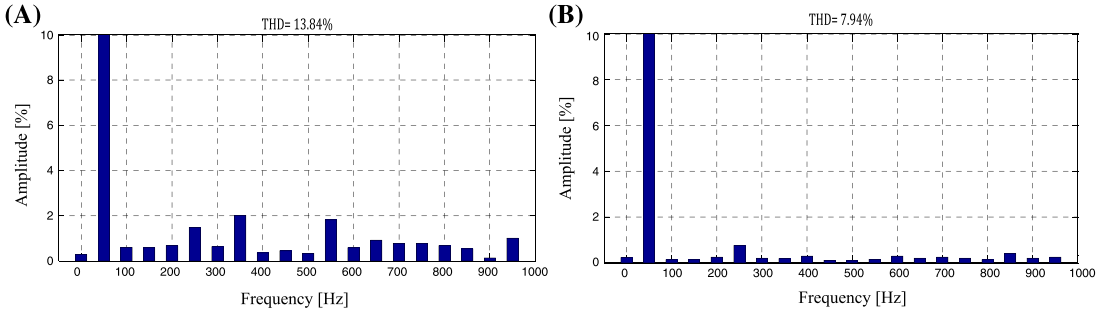


**FIGURE 8** Spectrum of total harmonics distortion (THD) for stator phase current $i_{sa}$. **A**, for DTC. **B**, for PTC [Color figure can be viewed at wileyonlinelibrary.com]

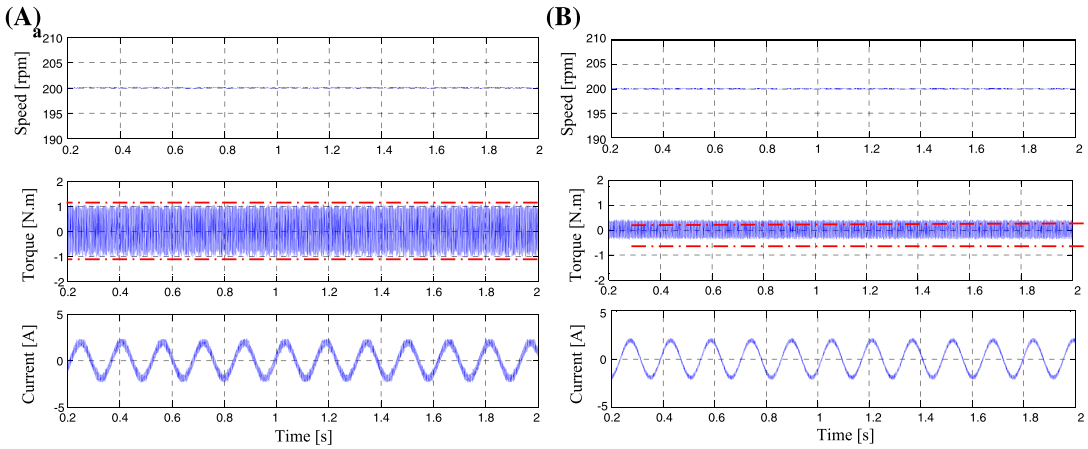


**FIGURE 9** Low speed operation: Rotor speed [rpm], torque [N.m], Stator phase current [a]. **A**, for DTC. **B**, for PTC [Color figure can be viewed at wileyonlinelibrary.com]

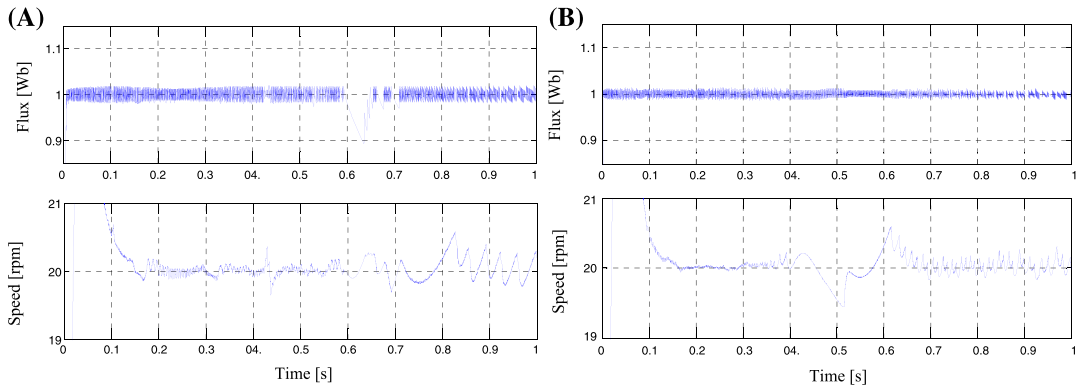


**FIGURE 10** Stator resistance $R_s$ variation test: Flux magnitude [Wb], rotor speed [rpm]. **A**, for DTC. **B**, for PTC [Color figure can be viewed at wileyonlinelibrary.com]

the low-speed range, even though they show good robustness in high and medium speed ranges. However, in the case of PTC strategy, the effect on flux magnitude was lower due to the optimization process.

## 4.3 | PI and TS-FLC speed controller performance analysis

This section exhibits the comparison of the performance of the predictive torque control strategy with the PI and the proposed Takagi-Sugeno speed controllers. The PI controller gains have been designed using the traditional method (poles placement), while the TS-FLC normalization are selected based on expert knowledge. The Figures are specified by (a) for PI and (b) for TS-FLC.

Figures 11–13 present comparative analysis of the PI and TS-FLC for the speed control in PTC scheme. Figure 11 shows the starting up and load application of 5 N.m. It can be observed that TS-FLC shows faster speed and torque responding. Moreover, TS-FLC has

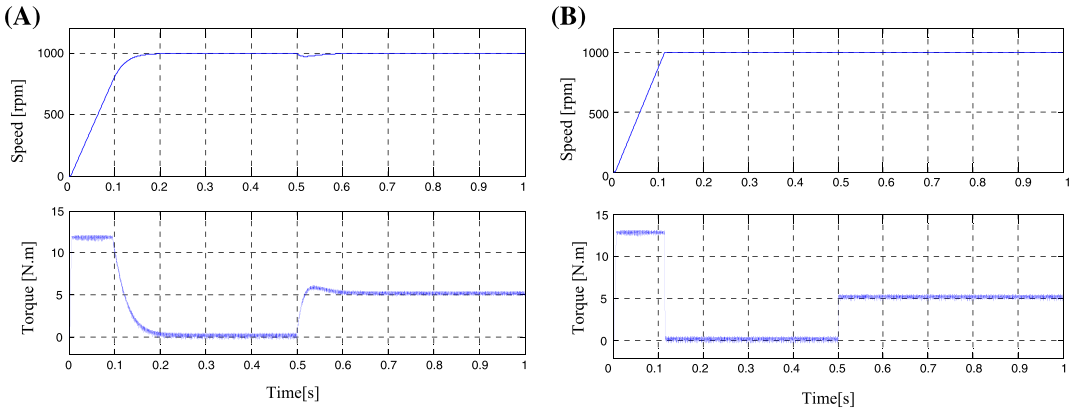


**FIGURE 11** Rotor speed [rpm], torque [N.m] during the transient and steady state with load application. **A**, for PI-PTC. **B**, for FLC-PTC [Color figure can be viewed at wileyonlinelibrary.com]

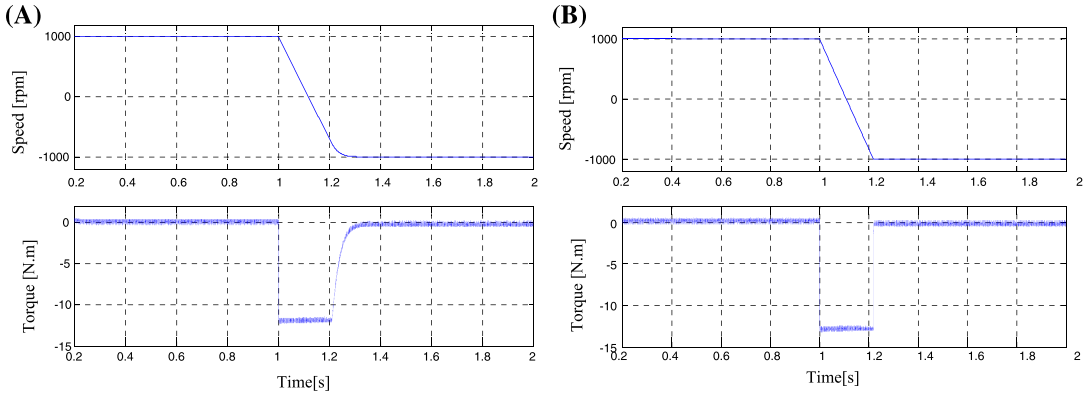


**FIGURE 12** Rotor speed [rpm], torque [N.m] during the speed reversal. **A**, for PI-PTC. **B**, for FLC-PTC [Color figure can be viewed at wileyonlinelibrary.com]

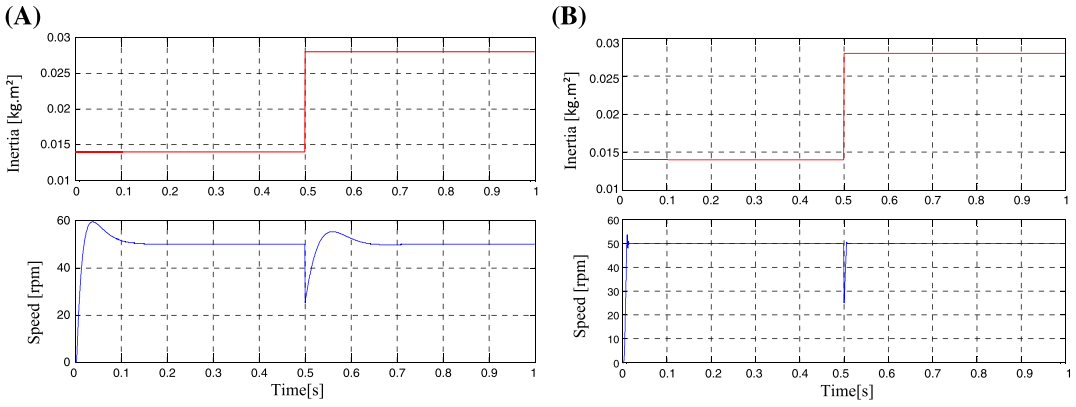


**FIGURE 13** Inertia variation test: Inertia moment [kg.m$^2$], rotor speed [rpm]. **A**, for PI-PTC. **B**, for FLC-PTC [Color figure can be viewed at wileyonlinelibrary.com]

not been affected by load disturbance, which reflects its high robustness. In contrast, the PI shows a vulnerable response in which speed dropping is noticeable. Next, in Figure 12, a speed sense reversing test has been done, and it can be seen that TS-FLC in Figure 12(b) provides a shorter responding time during reversing than PI in Figure 12(a). Figure 13 presents a perturbation introduction test in order to check the robustness of PI and TS-FLC speed controllers. This test consists of sudden inertia moment variation by *100%* at *0.5 s* in the low-speed region of *50 rpm* (*5.23 rad/s*). In Figure 13 (a), a significant effect of inertia variation appears on the speed response in the case of the PI controller, where the speed shows a huge undershoot before the

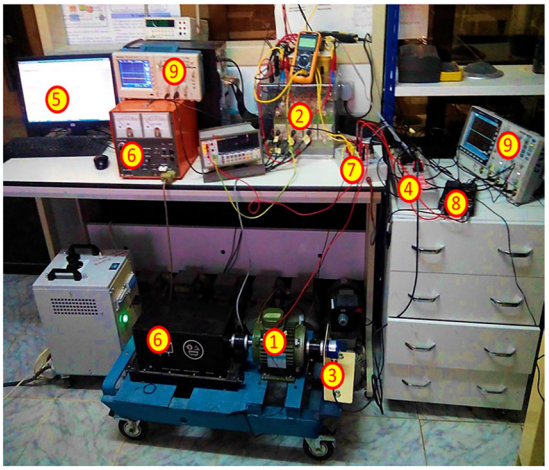

**FIGURE 14** Presentation of the experimental setup [Color figure can be viewed at wileyonlinelibrary.com]

PI starts recovering from speed dropping. However, in Figure 13(b), the TS-FLC has not shown a considerable influence, where the speed dropping has been recovered quickly, which confirm the high robustness and disturbance rejection ability of TS-FLC.

## 5 | EXPERIMENTAL VALIDATION

The experimental results are obtained with the aid of the software/hardware interface dSpace 1104. The experimental test bench of IM drive is composed as presented in (Figure 14) of: (i) a squirrel-cage IM; (ii) power electronics Semikron IGBT inverter; (iii) incremental encoder; (iv) dSpace 1104; with (v) MATLAB/Simulink software; (vi) magnetic powder brake with the load control unit; (vii) Hall effect current sensors; (viii) DC-bus voltage sensor; and (ix) digital oscilloscope.

### 5.1 | ST-DTC and PTC comparative analysis

This section presents the same operation tests as displayed in the simulation section. The Figures are

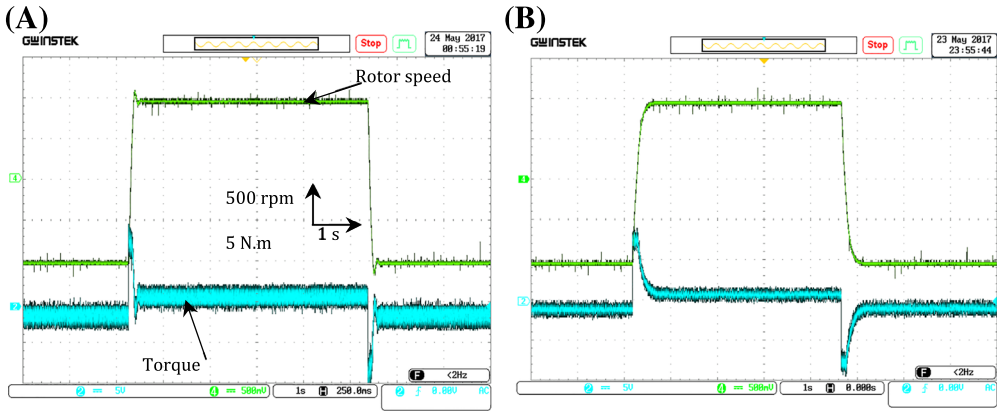


**FIGURE 15** Rotor speed and torque responses as a reversal maneuver. **A**, for DTC. **B**, for PTC [Color figure can be viewed at wileyonlinelibrary.com]

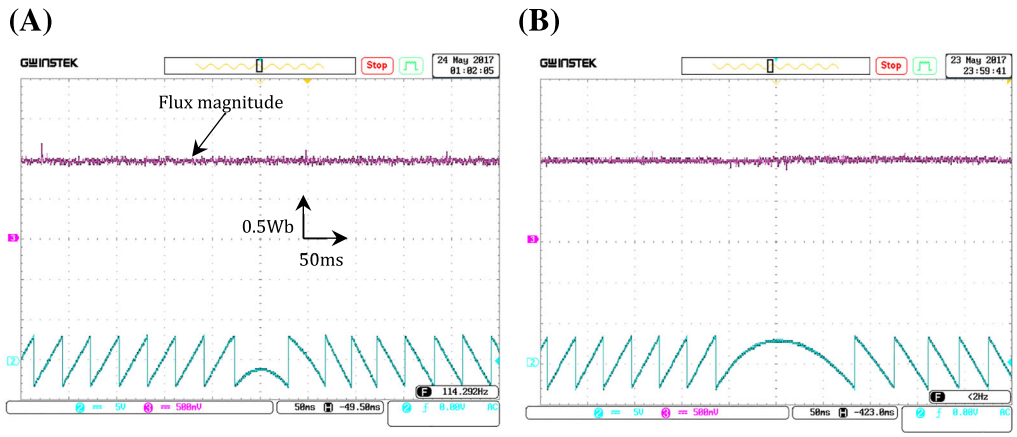


**FIGURE 16** Stator flux magnitude and position during the reversal maneuver. **A**, for DTC. **B**, for PTC [Color figure can be viewed at wileyonlinelibrary.com]

specified by (a) for switching table-based DTC (ST-DTC) and (b) for predictive torque control (PTC).

The first conducted test in Figure 15 shows speed and torque responses during rotation sense reversing. It can be seen in Figure 15(b) that the predictive torque control (PTC) provides a considerable reduction in torque ripples compared to ST-DTC. Next, in Figure 16, the stator flux magnitude and position are illustrated. The experimental results show that PTC reduces the flux ripples also. The depicted results in Figure 17 illustrate the flux components and the stator phase current, where it can be seen that the traditional DTC in Figure 17(a) presents a distorted form of flux and current. In contrast the PTC in Figure 17(b) presents a smoother waveform and lower current harmonics. Then in Figure 18, the load application of 5 N.m has been done. It can be seen that PTC provides a better current waveform and an important reduction in torque ripples. In Figure 19, the low-speed operation test has been performed. The motor operates with a rotor speed of *200 rpm* without load. The Figures show from top to bottom, speed, torque, and current. In Figure 19(a), the rotor speed shows some fluctuations while the torque ripples of DTC have been increased (±2 N.m) and its waveform has been deformed. On the other hand, the model predictive control-based technique in Figure 19(b) preserves a good behavior, better current quality, and reduced torque ripples level (±0.5 N.m) at the low-speed region.

## 5.2 | PI and FLC speed controller performance analysis

This section exhibits a comparison of PI and TS-FLC in the external speed loop of PTC strategy as presented in the simulation section. The Figures are specified by (a) for PI and (b) for FLC.

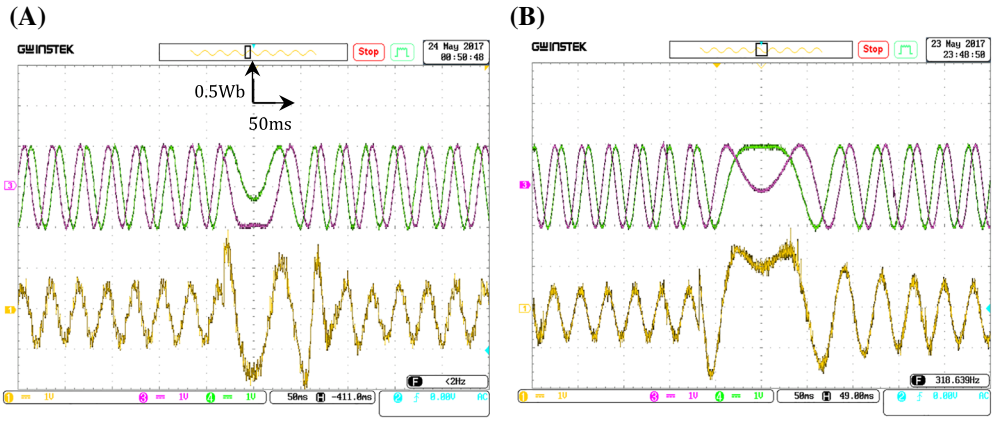


**FIGURE 17** Stator flux components and stator current during the sense reversal. **A**, for DTC. **B**, for PTC [Color figure can be viewed at wileyonlinelibrary.com]

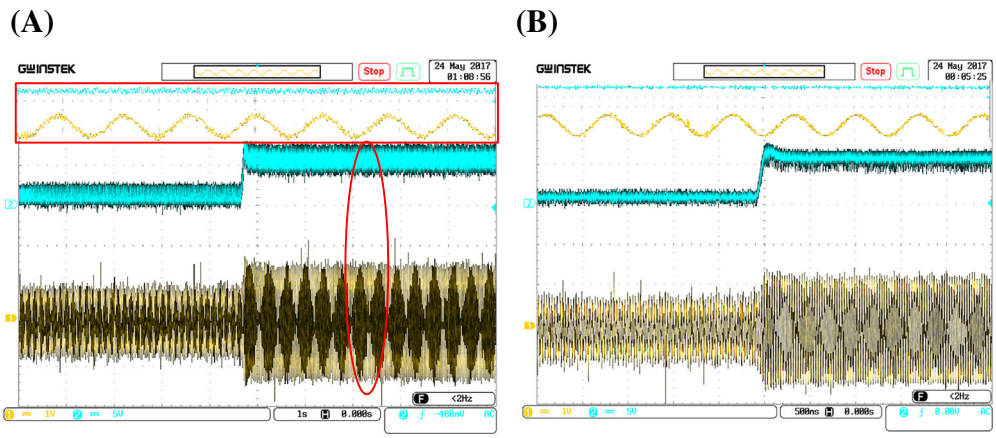


**FIGURE 18** Electromagnetic torque and stator current during load application. **A**, for DTC. **B**, for PTC [Color figure can be viewed at wileyonlinelibrary.com]

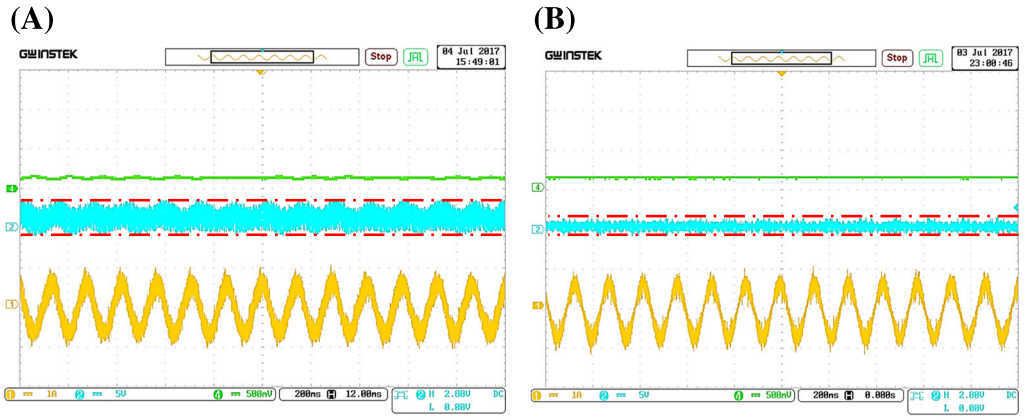


**FIGURE 19** Low speed operation: Rotor speed [rpm], torque [N.m], Stator phase current [a]. **A**, for DTC. **B**, for PTC [Color figure can be viewed at wileyonlinelibrary.com]

Figure 20 illustrates the rotor speed and torque in both cases (i.e., PI and TS-FLC). The TS-FLC in Figure 20(b) is much faster and is not particularly affected due to load disturbance contrary to the PI controller, which provides an important speed dropping. Furthermore, the torque response of TS-FLC is faster and has less overshoot. Then, in Figure 21 a reversal maneuver has been conducted. This test shows rotor speed and torque response with time determination. The revising time in case of PI is *320 ms* compared to *116 ms* in case of FLC, this difference reflects the significant rapidity of the Takagi-Sugeno fuzzy logic controller in the speed loop.

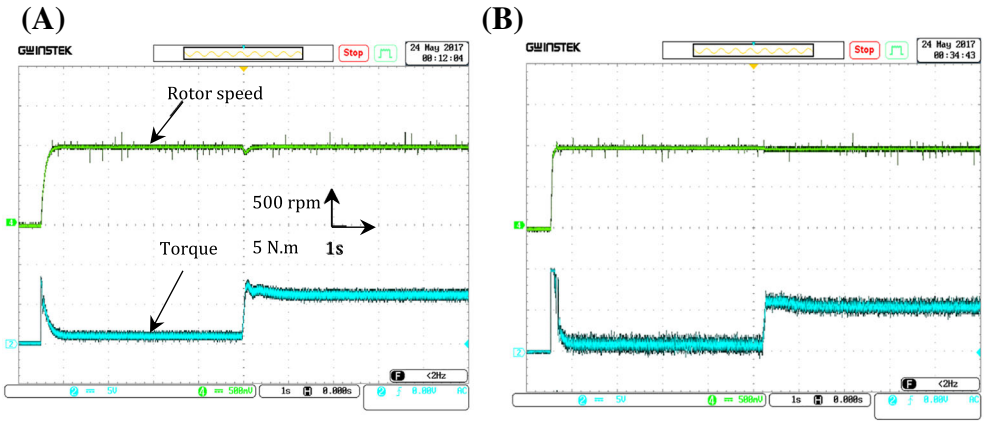


**FIGURE 20** Rotor speed and torque at starting up and load application [Color figure can be viewed at wileyonlinelibrary.com]

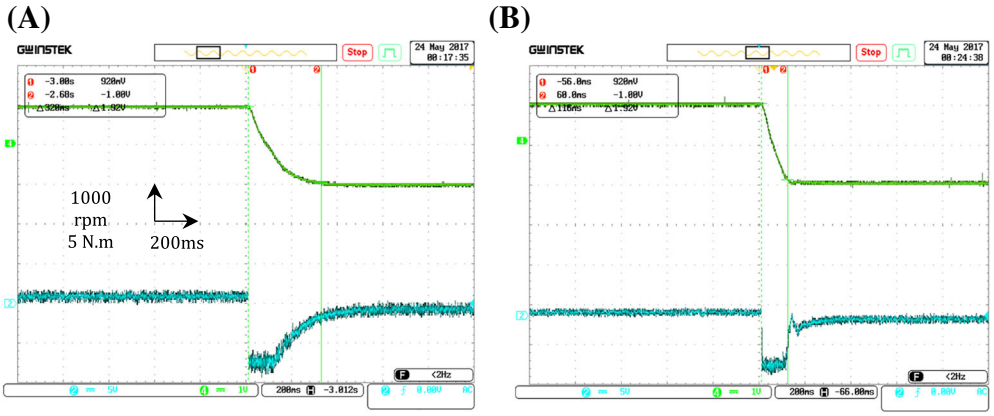


**FIGURE 21** Rotor speed and torque during the reversal maneuver [Color figure can be viewed at wileyonlinelibrary.com]

## 6 | CONCLUSIONS

This paper presents a performance enhancement of finite-state predictive torque control (FS-PTC) for induction motor drive. PTC control scheme has been associated with T-S fuzzy logic controller for speed regulation instead of the traditional PI controller. TS-FLC can offer good dynamic an accurate reference tracking without the need of a predefined model. Furthermore, it generates faster and precise torque reference torque for cost function design.

The presented control methods have been verified through simulation and experimental implementation using dSpace 1104 under different operation conditions. Despite its variable switching frequency, PTC offers reduced ripples and good current quality which can solve the main DTC drawbacks. Besides, the results indicate that the disturbance rejection ability has been improved when TS-FLC has been injected in the external loop of the PTC scheme. Conclusively, the high flexibility of the model predictive control design and the combination with artificial intelligence techniques as a complement make it able to handle different system constraints and overcome the shortcomings.

## REFERENCES


1. D. Casadei et al., *FOC and DTC: Two viable schemes for induction motors torque control*, IEEE Trans. Power Electron. **17** (2002), 779–787. https://doi.org/10.1109/TPEL.2002.802183.
2. J. Rodriguez et al., *Predictive current control of a voltage source inverter*, IEEE Trans. Ind. Electron. **54** (2007), 495–503. https://doi.org/10.1109/TIE.2006.888802.
3. M. Chebaani et al., *Sensorless finite-state predictive torque control of induction motor fed by four-switch inverter using extended Kalman filter*, COMPEL - Int. J. Comput. Math Electr. Electron. Eng. **37** (2018), 2006–2024. https://doi.org/10.1108/COMPEL-08-2017-0349.
4. P. Alkorta et al., *Efficient multivariable generalized predictive control for sensorless induction motor drives*, IEEE Trans. Ind. Electron. **61** (2014), 5126–5134. https://doi.org/10.1109/TIE.2013.2281172.
5. Ammar A, Kheldoun A, Metidji B, Talbi B, Ameid T, Azzoug Y. An experimental assessment of direct torque control and model predictive control methods for induction machine drive. IEEE International Conference on Electrical Sciences and Technologies in Maghreb (CISTEM); 2018: 1–6.
6. P. Correa, M. Pacas, J. Rodriguez, *Predictive torque control for inverter-fed induction machines*, IEEE Trans. Ind. Electron. **54** (2007), 1073–1079. https://doi.org/10.1109/TIE.2007.892628.
7. J. Wang et al., *Design and implementation of disturbance compensation-based enhanced robust finite control set predictive torque control for induction motor systems*, IEEE Trans. Ind. Inform. **13** (2017), 2645–2656. https://doi.org/10.1109/TII.2017.2679283.
8. M. M. El shormbably and A. Abido, *Efficient predictive torque control for induction motor drive*, IEEE Trans. Ind. Electron. **66** (2019), 6757–6767. https://doi.org/10.1109/TIE.2018.2879283.
9. M. Norambuena et al., *A very simple strategy for high-quality performance of AC machines using model predictive control*, IEEE Trans. Power. Electron. **34** (2019), 794–800. https://doi.org/10.1109/TPEL.2018.2812833.
10. C. Garcia et al., *Full predictive cascaded speed and current control of an induction machine*, IEEE Trans. Energy. Convers. **31** (2016), 1059–1067. https://doi.org/10.1109/TEC.2016.2559940.
11. H. Hamdi et al., *Fault diagnosis based on sliding mode observer for LPV descriptor systems*, Asian J. Control. **21** (2019), 89–98. https://doi.org/10.1002/asjc.2022.
12. M. Hoshyar and M. Mola, *Full adaptive integral backstepping controller for interior permanent magnet synchronous motors*, Asian J. Control. **20** (2018), 768–779. https://doi.org/10.1002/asjc.1616.
13. S.-A. Touil et al., *A sliding mode control and artificial neural network based MPPT for a direct grid-connected photovoltaic source*, Asian J. Control. (2019), 1–14. https://doi.org/10.1002/asjc.2007.
14. S. Y. Wang, C. L. Tseng, C. J. Chiu, *Online speed controller scheme using adaptive supervisory TSK-fuzzy CMAC for vector controlled induction motor drive*, Asian J. Control. **17** (2015), 569–581. https://doi.org/10.1002/asjc.798.
15. S. Gómez-Peñate et al., *Sensor fault diagnosis based on a sliding mode and unknown input observer for takagi-sugeno systems with uncertain premise variables*, Asian J. Control. **21** (2019), 339–353. https://doi.org/10.1002/asjc.1913.
16. F. Wang et al., *Model-based predictive direct control strategies for electrical drives: An experimental evaluation of PTC and PCC methods*, IEEE Trans. Ind. Inform. **11** (2015), 671–681. https://doi.org/10.1109/TII.2015.2423154.
17. B. Talbi et al., *A high-performance control scheme for photovoltaic pumping system under sudden irradiance and load changes*, Sol. Energy, **159** (2018), 353–368. https://doi.org/10.1016/j.solener.2017.11.009.
18. A. Ammar, *Performance improvement of direct torque control for induction motor drive via fuzzy logic-feedback linearization*, COMPEL – Int. J. Comput. Math Electr. Electron Eng. COMPEL-04-2018-0183, (2019), https://doi.org/10.1108/COMPEL-04-2018-0183.

## APPENDIX A

The parameters of the squirrel-cage induction motor, employed for the simulation and the experimental implementation, in SI units are:

1.1 KW, 50 HZ, $P = 2$, $R_S = 6.75\ \Omega$, $R_R = 6.21\ \Omega$, $L_S = L_R = 0.5192$ H, $M_{SR} = 0.4957$ H, $F = 0.002$ N·M·S/RAD, $J = 0.01240$ KG·M$^2$

The sampling frequency:10 kHz.

The average inverter's switching frequency: 5 kHz.

DC link voltage: *Vdc = 537 V*.

The different control gains of simulation and experimental implementation:

| Controller | Gains values |
|---|---|
| Flux hysteresis controller bandwidth | ± 0.005 Wb |
| Torque hysteresis controller bandwidth | ±0. 05 N·m |
| PI speed controller | $K_p = 0.1$; $K_i = 0.234$ |
| TS-FLC normalization factors | $K_e = 0.005$; $K_{\Delta e} = 0.001$; $K_u = 50$ |